RSC Advances

PAPER

View Article Online
View Journal | View Issue

Cite this: *RSC Adv.*, 2023, **13**, 7413

Optimal preparation of a core–shell structural magnetic nanoadsorbent for efficient tetracycline removal

Xinyu Zheng, *[ab] Cong Shen,[a] Yongfu Guo [a] and Huaili Zheng [b]

As emerging contaminants, tetracyclines pose a severe threat to aquatic environments and human health. Therefore, developing efficient approaches to remove tetracyclines from water has attracted a large amount of interest. Herein, a novel core–shell structural magnetic nanoadsorbent (FSMAS) was facilely prepared by graft copolymerization of acrylamide (AM) and sodium *p*-styrene sulfonate (SSS) monomers on the surface of vinyl-modified Fe_3O_4@SiO_2 (FSM). From single factor experiments, the optimal graft copolymerization conditions were concluded to be the following: initiator concentration = 1.2‰, reaction pH = 9, monomer molar ratio = 7 : 3. The surface morphology, microstructure and physicochemical properties of as-prepared FSMAS were fully evaluated by different characterization techniques, including SEM, TEM, FTIR, XPS, XRD and VSM. The adsorption performance of FSMAS towards tetracycline hydrochloride (TCH) was systematically studied by batch adsorption experiments. Results showed that the adsorption capability of the adsorbent was largely enhanced after graft copolymerization. The removal rate of TCH by FSMAS reached 95% at solution pH = 4.0, almost 10 times higher than FSM. Besides, the adsorption process of TCH by FSMAS was very efficient, 75% of pollutant could be adsorbed after only 10 minutes, attributed to the stretch of polymer chains and the strong affinity provided by abundant functional groups. Furthermore, TCH-loaded FSMAS was easily regenerated with HCl solution, the regeneration rate was higher than 80% after five adsorption–desorption cycles. Superior adsorption capability, fast solid–liquid separation speed and satisfactory reusability demonstrated the great potential of FSMAS in practical tetracycline removal.

Received 31st December 2022
Accepted 28th February 2023

DOI: 10.1039/d2ra08331k

rsc.li/rsc-advances

1. Introduction

Recently, antibiotics have been frequently detected in ground water, surface water, and even drinking water.[1,2] The accumulation of antibiotics in the water system has persistent toxicity to aquatic organisms, causes disturbance in the human microbiome, and increases the antibiotic resistance of bacteria, therefore it poses severe public health risks.[3,4] With the progress of society and improvement of living standards, the public demand higher water quality. Governments worldwide have supported more research on developing efficient removal techniques for such emerging pollutants. Among various antibiotics, tetracyclines (TCs) are commonly used in human medicine and animal husbandry to treat continuous infection and boost livestock growth, respectively.[5] However, due to the limited metabolism in living organisms, the majority of TCs is excreted into the water environment through urine and feces.[6] Long-term intake of water polluted by TCs will cause a series of health problems, such as liver injury, gastrointestinal discomfort, bacterial breeding, and so on.[7,8]

Adsorption is considered as one of the most promising techniques to eliminate hazardous pollutants from water as it is cost-effective, easy to operate and efficient even at very low initial pollutant concentrations, *e.g.*, trace levels.[4,9,10] During the application of adsorption technique, selecting a suitable adsorbent is the most important step. The commonly used adsorbents for the removal of TCs include graphene oxide,[11] activated carbon,[12] zeolite-based composites,[13] nanomaterials,[14] organic polymers,[15] and so on. Owing to the disadvantages of some conventional adsorbents, such as poor adsorption capability and bad separation ability, it is still very meaningful and attractive for researchers to develop novel adsorbents with low cost, satisfactory removal performance, fast solid–liquid separation speed and easy reusability.

Since the 21st century, nanotechnology has played an important role in developing highly efficient water treatment materials.[16,17] By decreasing the particle size to nanoscale, magnetic nanomaterials have a remarkably increased specific surface area, which provides more contact opportunities to target pollutants.[18] Furthermore, magnetic nanomaterials can

[a]*Jiangsu Provincial Key Laboratory of Environmental Science and Engineering, Suzhou University of Science and Technology, Suzhou 215009, China. E-mail: xinyuzheng@mail.usts.edu.cn*

[b]*Key Laboratory of the Three Gorges Reservoir Region's Eco-Environment, State Ministry of Education, Chongqing University, Chongqing 400045, China*

be easily separated from water because of its unique magnetic responsiveness, thus shortening the treatment time, decreasing the separation cost, and ensuring the subsequent regeneration.[18] Among different magnetic nanomaterials, Fe_3O_4 magnetic nanoparticles (MNPs) are recognized as promising adsorbents for various pollutants, due to their low toxicity, facile preparation and reasonable price.[5] However, bare Fe_3O_4 MNPs generally suffer from drawbacks of poor acid resistance, easy agglomeration and limited adsorption sites.[19,20] Therefore, improving the stability and adsorption ability of Fe_3O_4 MNPs by proper modification and functionalization are essential steps before their application.[21] One common modification way is to coat the Fe_3O_4 MNPs with a protective shell. Silicon dioxide (SiO_2) has good chemical stability, thereby can be served as the protective shell to isolate acid and oxygen.[22] In addition, the biocompatibility of SiO_2 is beneficial for further functionalization. Binyan Huang *et al.*[23] prepared Fe_3O_4@SiO_2–chitosan/GO nanocomposite and tested its adsorption ability for tetracycline from aqueous environments, the highest adsorption capacity was 67.57 mmol kg^{-1}. Wanling Cai *et al.*[24] studied the adsorption process of doxorubicin hydrochloride on glutaric anhydride functionalized Fe_3O_4@SiO_2 magnetic nanoparticles. Zhengwen Wei *et al.*[20] found that Fe_3O_4–SiO_2–dimethoxydiphenylsilane nanocomposite exhibited an excellent adsorption performance for phenanthrene, the removal efficiency improved 98.16% after coating and functionalization.

Anionic polyacrylamide P(AM-SSS) is copolymerized by acrylamide (AM) monomer and sodium *p*-styrene sulfonate (SSS) monomer, has been proved to be an effective flocculant for hematite wastewater treatment.[25] With abundant negative charges, numerous functional groups and flexible polymer chains, P(AM-SSS) has great potential to rapidly attract and firmly grab TC pollutants. Therefore, we tried to synthesize a core–shell structural magnetic nanoadsorbent with Fe_3O_4@SiO_2 as the magnetic core (strengthen solid–liquid separation ability) and anionic polyacrylamide P(AM-SSS) as the functionalized polymer shell (strengthen TC adsorption ability). To the best of our knowledge, there is no report about the relevant study at present yet.

Herein, a novel core–shell structural magnetic nanoadsorbent named Fe_3O_4@SiO_2–MPS-*g*-P(AM-SSS) (FSMAS) was facilely prepared by graft copolymerization of acrylamide (AM) and sodium *p*-styrene sulfonate (SSS) monomers on the surface of vinyl-modified Fe_3O_4@SiO_2 MNPs (Fe_3O_4@SiO_2–MPS), as shown in Scheme 1. The effects of initiator concentration, reaction pH, and monomer molar ratio on the graft copolymerization process were carefully investigated to obtain the optimal copolymerization conditions. The morphology, structure, physiochemical properties and magnetization intensity of FSMAS were fully characterized by various characterization techniques. The adsorption behaviors of as-prepared FSMAS towards tetracycline hydrochloride (TCH) under different adsorption conditions, including solution pH, adsorption time and adsorbent dosage, were discussed in a series of batch adsorption experiments. Moreover, adsorption mechanism was proposed and adsorbent reusability was evaluated.

2. Materials and methods

2.1. Materials

All the reagents used in this study were of analytical grade. Acrylamide (AM), sodium *p*-styrene sulfonate (SSS), 3-

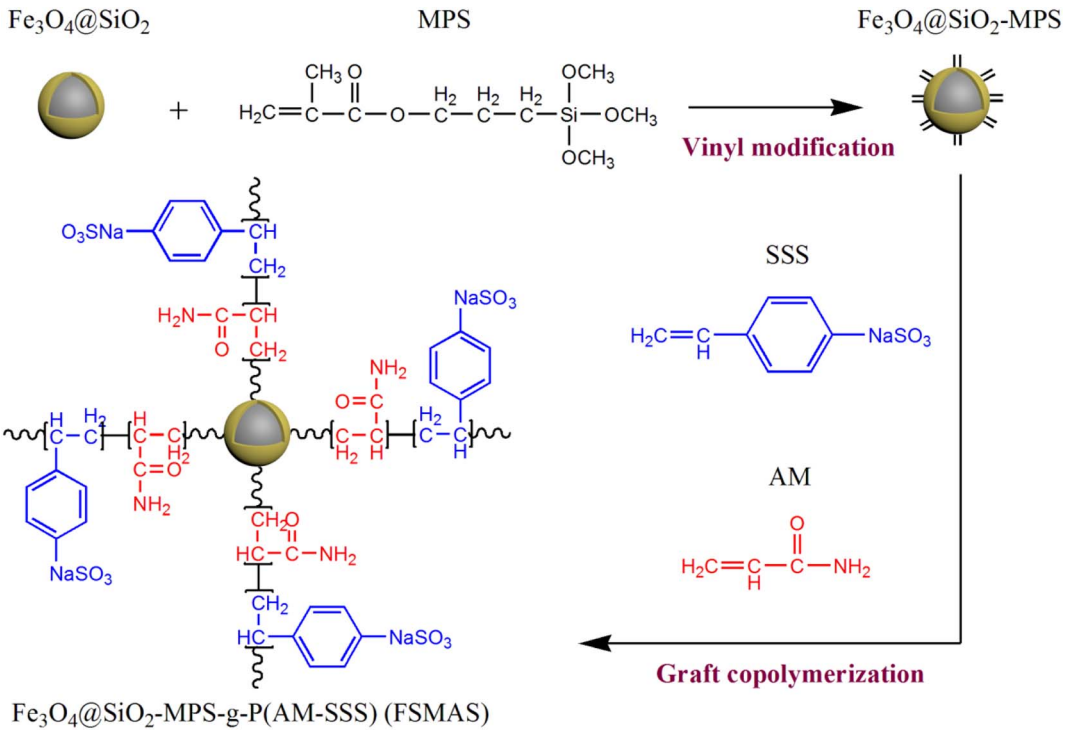

Scheme 1 Preparation of core–shell structural magnetic nanoadsorbent Fe_3O_4@SiO_2–MPS-*g*-P(AM-SSS) (FSMAS).

(trimethoxysilyl)propyl methacrylate (MPS), sodium hydroxide (NaOH), hydrochloric acid (HCl, 37wt%) and ammonium persulfate were purchased from Aladdin Reagent Co., Ltd. (Shanghai, China). Anhydrous ethanol (99.7% purity) and tetracycline hydrochloride (TCH) were supplied by Macklin Biochemical Technology Co., Ltd. (Shanghai, China). Deionized Milli-Q water (18 μS cm^{-1}) was used to prepare solutions.

2.2. Preparation of core–shell structural magnetic nanoadsorbent

2.2.1. Preparation of Fe_3O_4@SiO_2–MPS (FSM). Fe_3O_4 and Fe_3O_4@SiO_2 were pre-prepared by solvothermal method and Stöber method, respectively, as introduced in our previous researches.[10,26] In order to achieve a higher grafting efficiency with organic monomers, abundant vinyl groups were introduced on the surface of Fe_3O_4@SiO_2 by silane coupling agent MPS. A certain amount of Fe_3O_4@SiO_2 and 200 mL anhydrous ethanol were added into a three-necked flask, and ultrasonically mixed for 10 minutes. The flask was then transferred into a 78 °C water bath pot, and deoxidized with pure N_2 for 15 minutes. Subsequently, 9% MPS–ethanol solution was added dropwise into the flask, and the vinyl modification was carried out under a constant mechanical stirring for 12 hours. Finally, Fe_3O_4@SiO_2–MPS was collected by magnetic separation, washed three times with anhydrous ethanol and deionized water, and dried completely in a freeze-dryer.

2.2.2. Preparation of Fe_3O_4@SiO_2–MPS-*g*-P(AM-SSS) (FSMAS). Fe_3O_4@SiO_2–MPS-*g*-P(AM-SSS) was prepared by graft copolymerization with ammonium persulfate as the initiator. Predetermined amounts of AM and SSS monomers were dissolved in 200 mL deionized water, and the solution pH was adjusted by 1 mol L^{-1} NaOH and 1 mol L^{-1} HCl. Subsequently, 0.68 g Fe_3O_4@SiO_2–MPS was ultrasonically dispersed in the above-prepared monomer solution and the mixture was poured into a 500 mL three-necked flask. After bubbling with pure N_2 for 20 minutes and adding a certain amount of initiator, the flask was sealed immediately and stirred mechanically at 65 °C. After a seven-hour copolymerization and a one-hour aging, FSMAS was obtained by magnetic separation, purified with anhydrous ethanol, and dried in a freeze-dryer for further use.

2.3. Characterization

The microscopic characteristics and surface morphology of the as-prepared nanoadsorbent were studied by transmission electron microscope (TEM) and scanning electron microscope (SEM). The crystallographic structure of magnetic materials was obtained from 2θ = 10–70° by X-ray powder diffractometer (XRD, Cu-Kα: λ = 1.54056 Å) at a scanning rate of 0.05° s^{-1}. Fourier transform infrared (FTIR) spectra of samples dispersed in potassium bromide pellets were recorded in the range of 4000–500 cm^{-1} by a FTIR spectrometer. X-ray photoelectron spectroscopy (XPS) analysis was performed by an XPS spectrometer with Al-Kα ray as the excitation source. Saturation magnetization values were determined by vibrating sample magnetometer (VSM) from a magnetic field range of −20 000 Oe to +20 000 Oe at room temperature. Zeta potential measurements (pH = 2–9) before and after graft copolymerization were carried out on a Zetasizer apparatus. Anionic quantity of the as-prepared nanoadsorbent was determined by colloidal back titration method with Toluidine blue as the indicator. The acid resistance of Fe_3O_4 and FSMAS was evaluated by measuring leaching concentration of Fe in different pH solutions by inductively coupled plasma-optical emission spectroscope (ICP-OES).

2.4. Adsorption experiments

Adsorption experiments of TCH by core–shell structural magnetic nanoadsorbent were carried out at room temperature and environmentally relevant concentration. The stock solution of TCH was prepared by dissolving tetracycline hydrochloride powder in deionized water to reach a concentration of 100 mg L^{-1}. The stock solution was stored at 4 °C in dark and diluted to 5 mg L^{-1} before use. Solution pH was adjusted by 1.0 mol L^{-1} HCl and 1.0 mol L^{-1} NaOH. The adsorption experiments were conducted by dosing different amounts of nanoadsorbent (0.25–2.00 g L^{-1}) into pollutant solutions in 100 mL amber glass bottles with Teflon caps. These bottles were enwrapped by aluminized paper to prevent photo-degradation and shaken in a thermostatic orbital shaker at 150 rpm.

After predetermined adsorption time, sample solution was taken out by magnetic separation and filtered using a 0.45 μm needle filter, which was pre-rinsed with sample solution to minimize filter adsorption. The initial and residual concentrations of TCH were analyzed by high performance liquid chromatography (HPLC). The removal rate (%) and adsorption capacity (q, mg g^{-1}) were calculated by eqn (1) and (2), respectively.

$$\text{Removal rate} = \left(1 - \frac{C_r}{C_i}\right) \times 100\% \quad (1)$$

$$q = \frac{(C_i - C_r) \times V}{m} \quad (2)$$

where C_i (mg L^{-1}) and C_r (mg L^{-1}) are the initial and residual concentrations of TCH, respectively, V (L) is the volume of TCH solution and m (g) is the mass of adsorbent.

2.5. Recycling experiments

After saturated adsorption, the TCH-loaded nanoadsorbent was taken out by magnetic separation, washed several times with deionized water, and immersed into 1 mol L^{-1} HCl solution for an excessive time. After that, the regenerated nanoadsorbent was neutralized with diluted NaOH solution and deionized water, dried in a freeze-dryer, and reused in the next adsorption–desorption cycle. The adsorption–desorption process was repeated for five times.

3. Results and discussion

3.1. Characterization

The microscopic characteristics and surface morphology of Fe_3O_4 and FSMAS were characterized by SEM and TEM, as

shown in Fig. 1. Fe_3O_4 sphere with a uniform particle size of about 600 nm was consisted by numerous Fe_3O_4 nanoballs (Fig. 1a), which was a general characteristic when Fe_3O_4 was prepared by solvothermal method.[27] The SEM image of FSMAS (Fig. 1b) looked more blurry than that of Fe_3O_4 (Fig. 1a), this was attributed to the existence of anionic polyacrylamide with low density and amorphous structure. The smoother surface of FSMAS than Fe_3O_4 also indicated the existence of anionic polyacrylamide. After coating and grafting processes, FSMAS was observed to have a clear core–shell structure with shell thickness of about 85 nm (Fig. 1d), inferring the successful modification by SiO_2 and functionalization by organic copolymer.

The FTIR spectra of Fe_3O_4, Fe_3O_4@SiO_2, FSM and FSMAS were illustrated in Fig. 2a. The strong peak presented in all spectra at 574 cm^{-1} was corresponded to the Fe–O stretching vibration,[28] indicating that Fe_3O_4 was successfully embedded into the core of nanoadsorbent. Due to the modification by SiO_2 layer, peak attributed to the Si–O–Si bending vibration at 1085 cm^{-1} was observed in Fe_3O_4@SiO_2, FSM, and FSMAS spectra.[29] Compared with FSM spectrum, new peaks for FSMAS spectrum at 1183 cm^{-1} and 1039 cm^{-1} were assigned to the sulfonic acid group of SSS monomer, peaks at 778 cm^{-1} and 679 cm^{-1} related to benzene ring were also characteristic peaks of SSS monomer.[25,26,30] In addition, peaks at 2935 cm^{-1} and 1453 cm^{-1} were respectively assigned to the methyl group and methylene group of AM monomer.[25] These characteristic peaks in FSMAS spectrum demonstrated the successful grafting of anionic polyacrylamide.

Surface elemental composition of FSM and FSMAS was analyzed by XPS, as shown in Fig. 2b. The missing element of Fe in both FSM and FSMAS spectra was due to the cover of SiO_2 layer. Strong peaks observed at 532.0, 284.6, 154.8, 103.8 and 25.1 eV were respectively corresponded to O 1s, C 1s, Si 2s, Si 2p and O 2s. Compared with FSM spectrum, new peaks for FSMAS spectrum at 399.8, 232.5 and 168.2 eV were respectively related to N 1s, S 2s and S 2p, revealing that abundant amino groups (–NH_2) and sulfonic acid groups (–SO_3^-) were existed in the self-made nanoadsorbent.

The XRD patterns of Fe_3O_4, Fe_3O_4@SiO_2, FSM and FSMAS were depicted in Fig. 2c. For all samples, seven reflection peaks were observed at $2\theta = 18.5°$, 30.5°, 35.7°, 43.4°, 53.6°, 57.3° and 62.8°, which were respectively assigned to the (111), (220), (311), (400), (422), (511), and (440) planes of face-centered cubic iron oxide phase. The XRD result confirmed that the size and crystal phase of Fe_3O_4 core were unchanged after SiO_2 coating and copolymer grafting.

The magnetic hysteresis curves of Fe_3O_4, Fe_3O_4@SiO_2, FSM and FSMAS were illustrated in Fig. 2d. The saturation magnetization values decreased from 80.36 emu g^{-1} (Fe_3O_4) to 52.25 emu g^{-1} (FSMAS) after modification and functionalization, owing to the introduction of nonmagnetic materials (*i.e.*, SiO_2, MPS and organic copolymer). Nevertheless, the saturation magnetization of FSMAS was sufficient to guarantee its magnetic separation from water, which was expected to shorten the water treatment time and decrease water treatment cost.

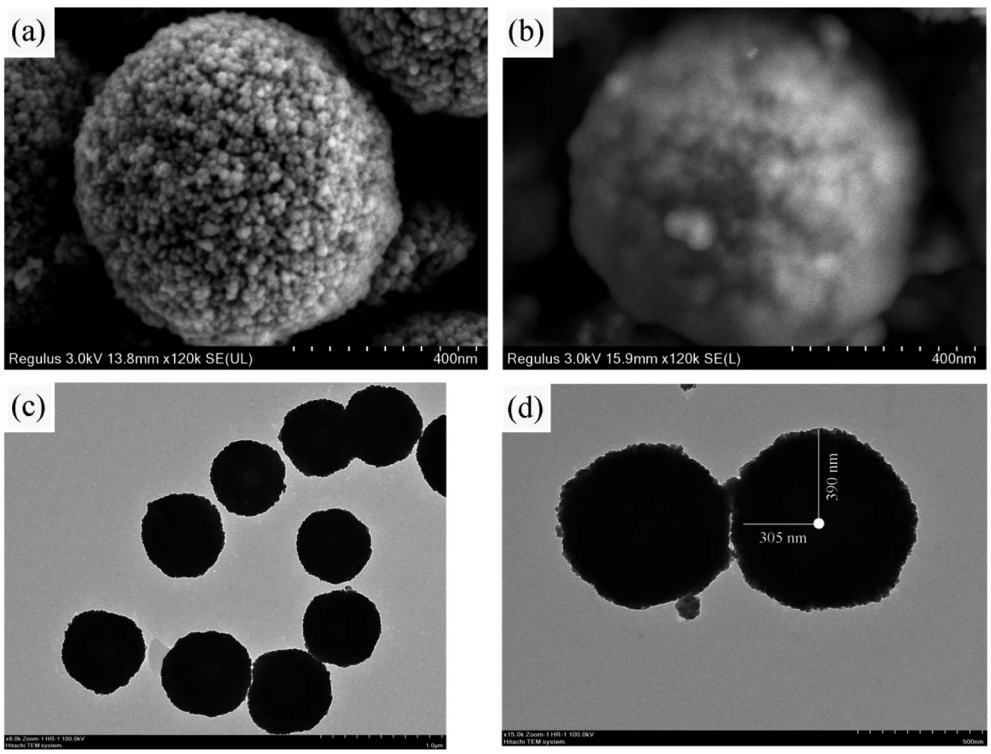

Fig. 1 SEM images of (a) Fe_3O_4 and (b) FSMAS; TEM images of (c) Fe_3O_4 and (d) FSMAS.

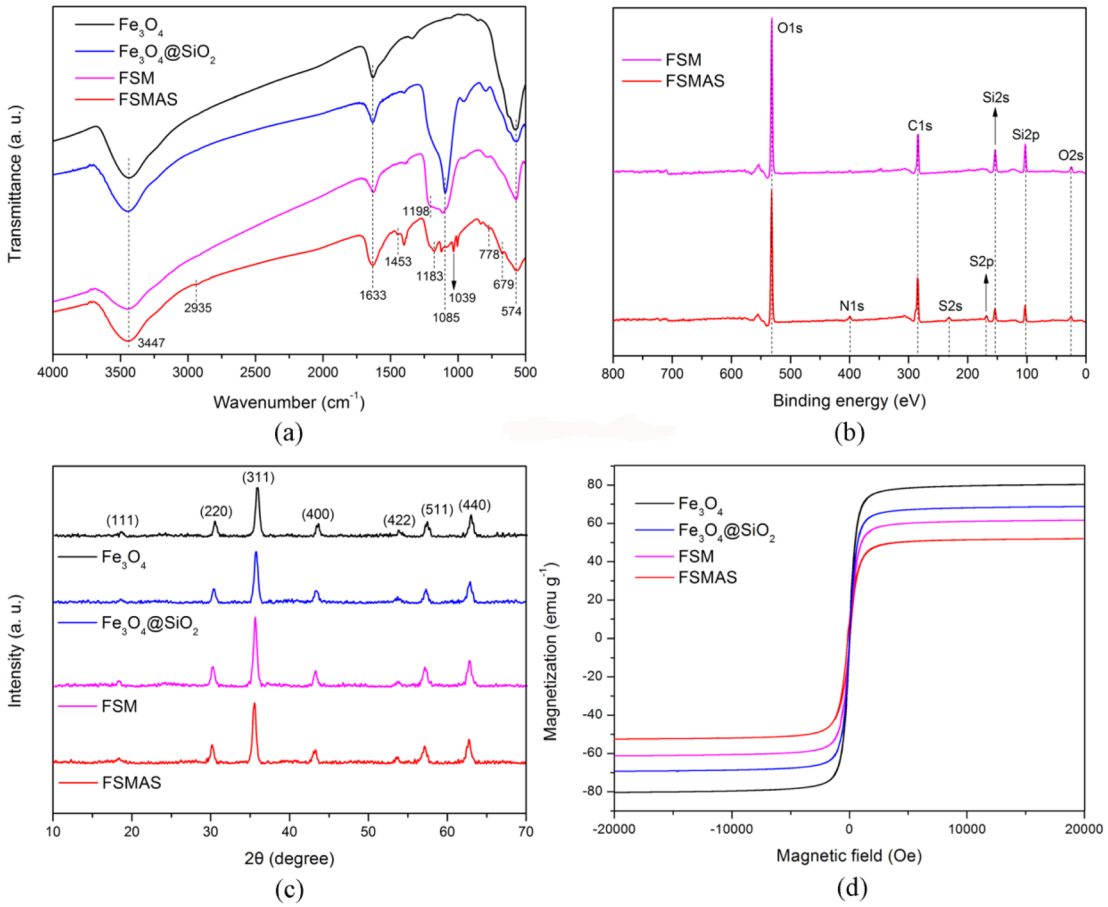

Fig. 2 Characterization: (a) FTIR spectra; (b) XPS spectra; (c) XRD patterns; and (d) magnetic hysteresis curves.

3.2. Optimization of graft copolymerization conditions

The adsorption ability of adsorbent generally depends on its structure and physicochemical properties. In this study, anionic quantity, which can reflect the affinity between anionic adsorbent and cationic pollutant, was selected as a representative property to estimate the adsorption performance of as-prepared FSMAS. The graft copolymerization process of AM and SSS monomers on vinyl-modified Fe_3O_4@SiO_2 followed the free radical polymerization mechanism, and could be divided into four stages, including chain initiation, chain growth, chain termination and chain transfer. Three key graft copolymerization conditions (*i.e.*, initiator concentration, reaction pH and monomer molar ratio) that affected the above-mentioned four stages were carefully discussed by single factor experiments, as shown in Fig. 3.

In chain initiation stage, the collision rate between monomers and initial free radicals was mainly depended on the initiator concentration. The effect of initiator concentration on anionic quantity of FSMAS was investigated at the total monomer concentration of 1 mol L^{-1}, monomer molar ratio of 9 : 1, and reaction pH of 10. Fig. 3a showed that the anionic quantity of FSMAS increased as the initiator concentration increased from 0.3‰ to 1.2‰, but declined rapidly with the further increase of initiator concentration. At a low initiator concentration, the small amount of initial free radicals inhibited the formation of monomer free radicals and further restrained chain growth. The "cage effect" resulted in an incomplete copolymerization and a low anionic quantity.[31] On the contrary, at a high initiator concentration, the fast collision rate increased the possibility of chain termination and chain transfer, also leading to a low anionic quantity.[32] Therefore, the optimal initiator concentration was 1.2‰.

The effect of reaction pH on anionic quantity of FSMAS was investigated at the total monomer concentration of 1 mol L^{-1}, monomer molar ratio of 9 : 1, and initiator concentration of 1.2‰. Fig. 3b showed that reaction pH also influenced the graft copolymerization process. When reaction pH was set at the range of 7–9, anionic quantity of FSMAS was obtained in a relatively high level of 0.052–0.064 mmol g^{-1}, indicating that proper alkalinity was beneficial to copolymerization of AM and AMPS on vinyl-modified Fe_3O_4@SiO_2. However, as the reaction pH further increased to 10 and 11, anionic quantity sharply decreased to 0.026 mmol g^{-1} and 0.022 mmol g^{-1}, respectively. At strong alkaline environment, the hydrolysis of AM monomer accelerated the production of nitrilopropionamide, which led to branch reaction and inhibited chain growth.[33] Therefore, the optimal reaction pH was selected to be 9.

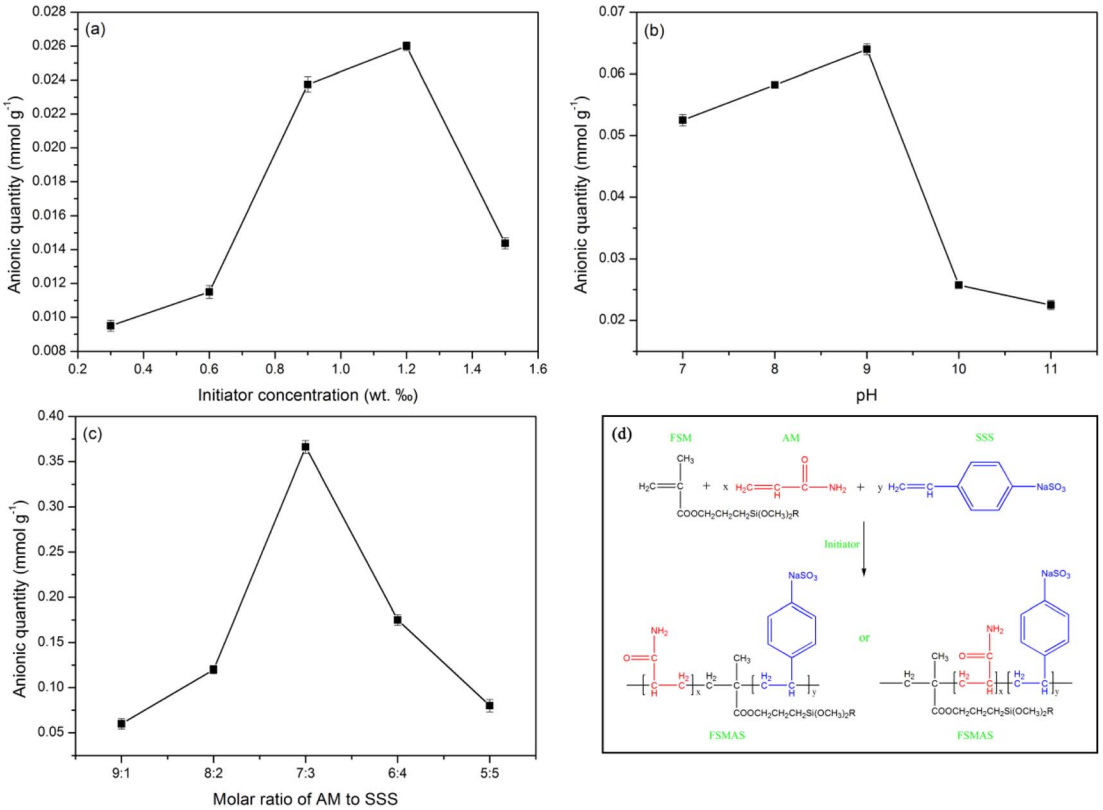

Fig. 3 Effects of graft copolymerization conditions on the anionic quantity of FSMAS: (a) initiator concentration; (b) reaction pH; (c) monomer molar ratio; and (d) proposed reaction routes.

The monomer molar ratio played the most important role in graft copolymerization process compared with the above-discussed two conditions. The effect of monomer molar ratio was investigated at the total monomer concentration of 1 mol L^{-1}, initiator concentration of 1.2‰, and reaction pH of 9. As shown in Fig. 3c, with the molar ratio of AM to SSS decreased from 9 : 1 to 7 : 3, anionic quantity significantly increased from 0.060 mmol g^{-1} to 0.366 mmol g^{-1}. However, with the further decrease of monomer molar ratio from 7 : 3 to 5 : 5, anionic quantity sharply declined. The lower anionic quantity of FSMAS at excessive AM molar percentage was due to the higher reactivity of AM than SSS. Excessive AM in system significantly increased copolymerization rate, released a large amount of heat that could not be dispersed in time, thereby leading to chain transfer and chain termination.[31] Excessive SSS also caused a lower anionic quantity of FSMAS, this could be explained by the increased electrostatic repulsion between SSS monomers, which led to a large steric hindrance and hampered the diffusion of the monomers to the surface of copolymer.[34] Besides, the relatively lower reactivity of SSS also inhibited chain growth. Therefore, the optimal monomer molar ratio of AM to SSS was deemed to be 7 : 3.

3.3. Adsorption of tetracycline hydrochloride

3.3.1. Effect of solution pH. Solution pH needs to be carefully adjusted before adsorption process because it significantly affects both existence form of adsorbate and surface charge of adsorbent. TCH is an amphoteric compound with three ionizable functional groups, corresponding to three pK_a values of 3.30, 7.68 and 9.69, its chemical structure is given in Fig. 4a. With the change of solution pH, these three functional groups can undergo protonation–deprotonation reactions and form cationic species TC^+, neutral species TC^0, anionic species TC^- and TC^{2-}, as depicted in Fig. 4b. Fig. 4c showed that in the whole tested pH range, the zeta potential of FSMAS was kept in a negative level, and was notably lower than the zeta potential of FSM. This phenomenon was due to the introduction of abundant sulfonic acid groups ($-SO_3^-$) by grafting SSS monomers.

In this study, the effect of solution pH on the adsorption performance of nanoadsorbent towards TCH was evaluated in a pH range of 2.0–9.0, with adsorbent dosage of 1 g L^{-1} and adsorption time of 240 minutes. The experimental results were illustrated in Fig. 4d. It was obvious that the removal rate of FSMAS was higher than that of FSM, especially in acid environment, demonstrating that the grafted P(AM-SSS) played a vital role in adsorption process. The synergistic reaction of polymer chains and functional groups of P(AM-SSS) provided numerous active adsorption sites to TCH, thereby significantly promoted adsorption.

With the increase of solution pH, the removal rate of FSMAS towards TCH firstly increased largely, and then decreased sharply, a maximum removal rate of 95% was obtained at pH = 4.0. In the pH range of 2.0–4.0, the dominated species of TCH

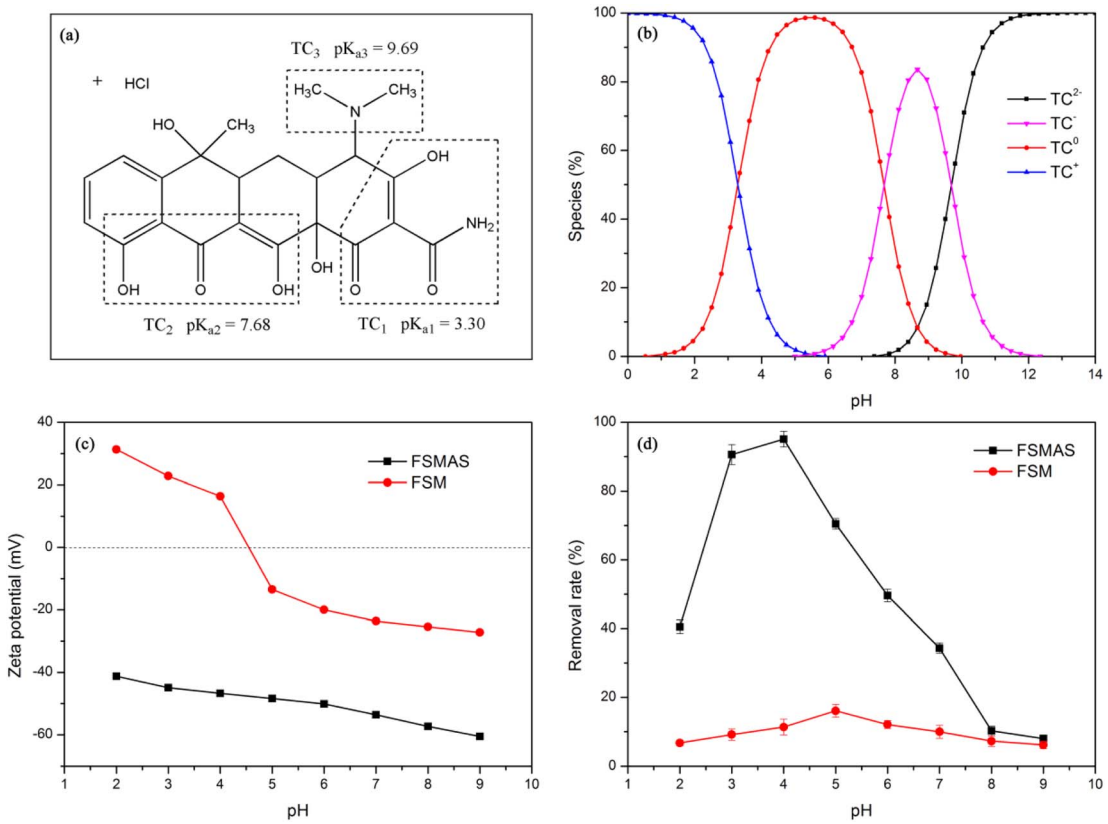

Fig. 4 (a) Chemical structure of TCH; effects of solution pH on (b) TC species; (c) zeta potential; and (d) removal rate.

were TC^+ and TC^0, accordingly the main attractive force between TCH and negatively charged FSMAS was electrostatic attraction. With the increase of solution pH in this range, the surface charge of FSMAS declined (Fig. 4c), thus provided stronger affinity to TCH. Besides, the competitive adsorption by hydrogen ions (H^+) also diminished at higher solution pH, therefore also leading to a better adsorption of TCH.

As solution pH increased to 5.0–7.0, TCH was mainly existed as TC^0 and TC^-. From the angle of electrostatic interaction and the consideration of net charge, TC^0 should not be attracted by FSMAS and TC^- should be repelled by FSMAS. However, the removal rate of FSMAS in this range was still significantly higher than that of FSM. This phenomenon was also observed by other researcher, probably due to the re-arrangement of TCH molecular structure, which let the positively charged group (–$NH(CH_3)_2^+$) located very close to the FSMAS surface and the negatively charged group as far as possible away from the surface.[35] It was also inferred that the simultaneous adsorbed H^+ could serve as the additional adsorption sites for neutral and negative TCH.[36] In addition, a stable π–π conjugated system could be formed by the π–π stacking interaction between the benzene rings of TCH and FSMAS, and hydrogen bonding could be found between amide group (–$CONH_2$) of FSMAS and hydroxy group (–OH) of TCH, which were also beneficial to the adsorption process at pH = 5.0–7.0.[30]

As the solution pH exceeded 8.0, the removal rate of FSMAS further declined and was very close to the removal rate of FSM, owing to that strong electrostatic repulsion between anionic FSMAS and anionic TCH weakened electrostatic interaction, π–π stacking interaction and hydrogen bonding.

3.3.2. Effect of adsorption time and adsorbent dosage. Adsorption rate reflects the application potential of a novel adsorbent. High adsorption rate can greatly shorten the water treatment time, thus reducing the water treatment cost. As shown in Fig. 5a, the removal of TCH by FSMAS was very fast at the initial stage of adsorption, the removal rate reached 75% after only 10 minutes, this was attributed to the strong affinity provided by flexible polymer chains and abundant functional groups of core–shell structural magnetic nanoadsorbent. Then, the removal rate increased slowly, owing to the consumption of both active adsorption sites and pollutant molecules. Finally, the adsorption process tended to reach equilibrium and a maximum removal rate of 95% was obtained. After adsorption, the magnetic nanoadsorbent could be separated from water within 10 seconds under the help of an external magnet, as shown in the inset of Fig. 5a, which guaranteed the subsequent regeneration.

The effect of adsorbent dosage on the adsorption process also needs to be carefully studied before practical application to find a balance between treatment performance and treatment cost. Fig. 5b showed that with the increase of adsorbent dosage from 0.25 g L^{-1} to 0.75 g L^{-1}, the removal rate of TCH by FSMAS increased sharply from 66% to 94%, but with the further increase of dosage, the removal rate increased slightly. At an

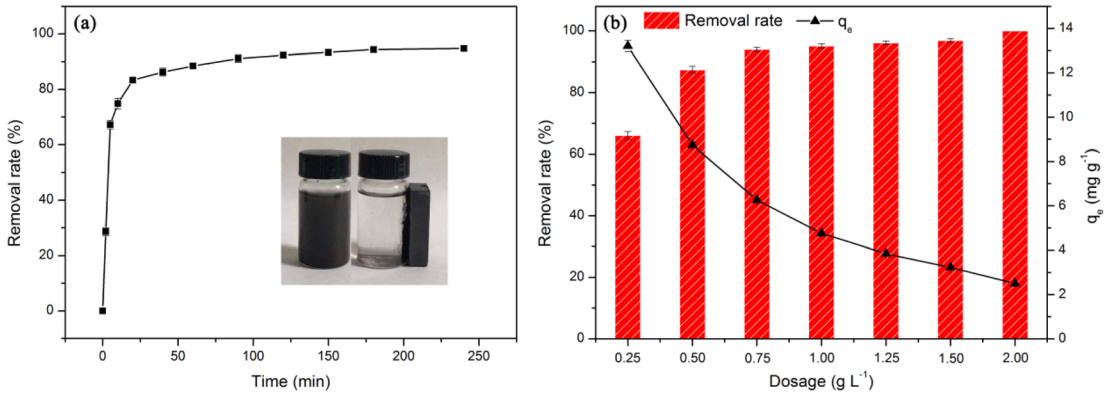

Fig. 5 Effects of (a) adsorption time and (b) adsorbent dosage on the adsorption process.

excessive dosage of 2.00 g L^{-1}, a 100% removal rate could be achieved. On the contrary, the adsorption capacity of TCH by FSMAS constantly decreased with the increase of adsorbent dosage. With a higher dosage, the TCH molecules in the solution were not enough to occupy all the adsorption sites on the FSMAS surface, causing an unsaturated adsorption and a waste of adsorbent. With the decrease of dosage, the amount of TCH molecules became relatively higher than that of adsorption sites, the increased "molecular pressure" promoted the fully use of adsorbent, thereby leading to a higher adsorption capacity.

3.3.3. Adsorption kinetics and isotherms. To better understand adsorption process, the time dependence of TCH adsorbed onto FSMAS was further analyzed at different TCH concentrations by two typical adsorption kinetic models (*i.e.*, pseudo-first-order (PFO) model and pseudo-second-order (PSO) model), as shown in eqn (3) and (4).

PFO model:

$$q_t = q_e(1 - e^{-k_1 t}) \quad (3)$$

PSO model:

$$q_t = \frac{k_2 q_e^2 t}{1 + k_2 q_e t} \quad (4)$$

where k_1 (min^{-1}) and k_2 (g mg^{-1} min^{-1}) are the PFO and PSO model rate constants, respectively, q_e (mg g^{-1}) and q_t (mg g^{-1}) are the adsorption capacity of FSMAS at equilibrium and different time interval, respectively.

The non-linear fitting curves of PFO and PSO models were shown in Fig. 6a and the corresponding parameters were summarized in Table 1. The correlation coefficient (R^2) values calculated with the PSO model (0.98175 and 0.97829) were higher than that calculated with the PFO model (0.97837 and 0.97802), and the theoretical q_e values of the PSO model (6.34 mg g^{-1} and 9.33 mg g^{-1}) were very close to experimental q_e values (6.31 mg g^{-1} and 9.22 mg g^{-1}). Therefore, the PSO model was more suitable to describe the adsorption process of TCH onto FSMAS.

In addition, the relationship between equilibrium adsorption capacity of FSMAS and equilibrium concentration of TCH was elaborated by two commonly used isotherm models (Langmuir and Freundlich), as shown in eqn (5) and (6), respectively.

Langmuir model:

$$q_e = \frac{C_e q_m K_L}{1 + C_e K_L} \quad (5)$$

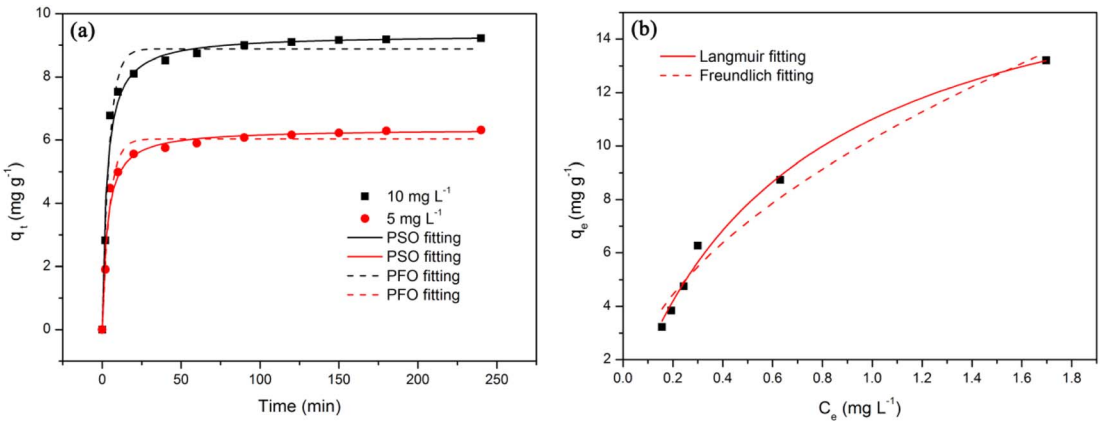

Fig. 6 (a) Adsorption kinetics of TCH adsorbed onto FSMAS; (b) adsorption isotherms of TCH adsorbed onto FSMAS.

Table 1 Kinetic parameters of TCH adsorbed onto FSMAS

TCH concentration (mg L^{-1})	$q_{e,exp}$ (mg g^{-1})	Pseudo first-order model			Pseudo second-order model		
		$q_{e1,cal}$ (mg g^{-1})	k_1 (min^{-1})	R^2	$q_{e2,cal}$ (mg g^{-1})	$k_2 \times 10$ (g mg^{-1} min^{-1})	R^2
5	6.31	6.03	0.22	0.97837	6.34	0.51	0.98175
10	9.22	8.88	0.23	0.97802	9.33	0.37	0.97829

Freundlich model:

$$q_e = K_F C_e^{1/n} \quad (6)$$

where q_m (mg g^{-1}) is the maximum adsorption capacity of FSMAS, K_L (L mg^{-1}) and K_F ($mg^{(1-1/n)}$ $L^{1/n}$ g^{-1}) are the Langmuir model and Freundlich model constants, n is the Freundlich model heterogeneity factor.

The non-linear fitting curves of Langmuir and Freundlich models were depicted in Fig. 6b and the corresponding parameters were listed in Table 2. Fig. 6b showed that the experimental data fitted well with the Langmuir model. Besides, the R^2 value of Langmuir model (0.99072) was higher than that of Freundlich model (0.96622), also indicating that the adsorption of TCH onto FSMAS was more suitable to describe with the Langmuir model.

3.3.4. Adsorption mechanism. Based on the above discussion, the adsorption of TCH by core–shell structural magnetic nanoadsorbent was described as following: (1) with a negative surface charge, the polymer chains of FSMAS stretched in solution by electrostatic repulsion, exposing numerous active adsorption sites for target pollutant; (2) abundant functional groups (*i.e.*, sulfonic acid groups, benzene rings and amide groups) of FSMAS provided strong affinity to target pollutant through electrostatic interaction, π–π stacking interaction and hydrogen bonding; (3) after fully loading target pollutant, the magnetic core of FSMAS helped to accelerate solid–liquid separation under an external magnetic field. The adsorption mechanism of TCH by core–shell structural magnetic nanoadsorbent at different solution pH was depicted in Fig. 7.

3.4. Recycling of TCH-loaded nanoadsorbent

From the point of cost-benefit analysis, the regeneration ability of a novel adsorbent needs to be confirmed to promote its large-scale application. The lower adsorption performance of FSMAS at pH = 2.0 (Section 3.3.1) suggested that it could be regenerated by acid pickling. Before regeneration, the acid resistance of FSMAS was evaluated by measuring leaching concentration of Fe in different pH solutions by ICP-OES. As shown in Fig. 8a, the leaching of Fe from FSMAS was inhibited even in extremely acid environment, whereas bare Fe_3O_4 presented a large Fe loss of 77% at pH = 0, indicating SiO_2 shell and grafted polymer played important roles in strengthening acid resistance of iron-based materials.

Herein, 1 mol L^{-1} HCl solution was served as the desorption agent to regenerate TCH-loaded FSMAS, and the adsorption–desorption performance in five cycles was shown in Fig. 8b. The

Table 2 Isothermal parameters of TCH adsorbed onto FSMAS

Langmuir model			Freundlich model		
q_m (mg g^{-1})	K_L (L mg^{-1})	R^2	n	K_F ($mg^{(1-1/n)}$ $L^{1/n}$ g^{-1})	R^2
18.51	1.46	0.99072	1.92	10.25	0.96622

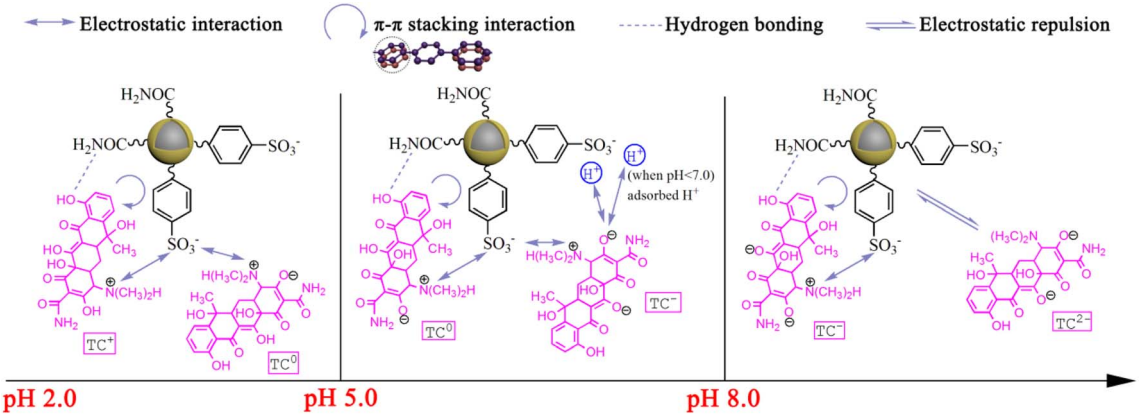

Fig. 7 Adsorption mechanism of TCH by core–shell structural magnetic nanoadsorbent at different solution pH.

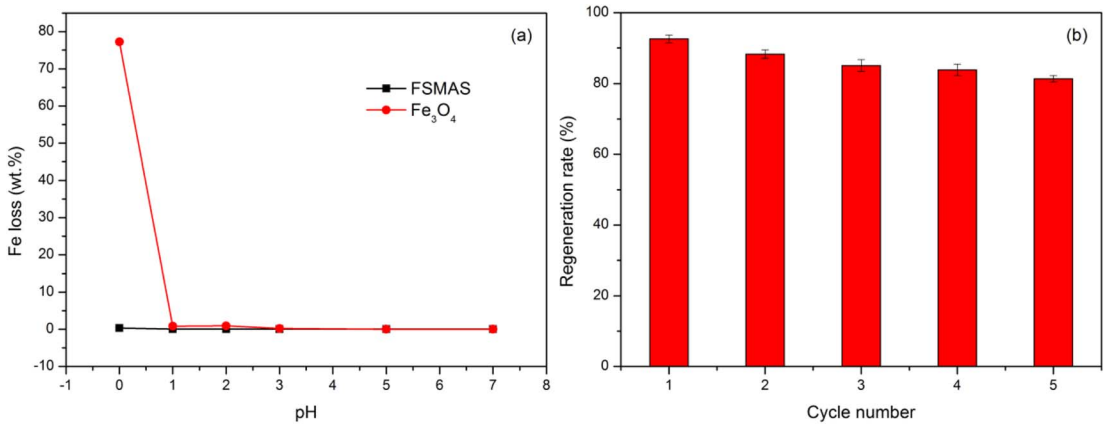

Fig. 8 (a) Comparison of Fe loss between FSMAS and Fe_3O_4 in different pH solutions and (b) regeneration rate of FSMAS in five adsorption–desorption cycles.

Table 3 Comparison of adsorption performance towards TCs between FSMAS and other reported adsorbents

Adsorbent	TC concentration (mg L^{-1})	Adsorbent dosage (g L^{-1})	Adsorption time (min)	Removal rate (%)	Separation method and time	Recycling	Reference
Graphene oxide	8.33	0.181	15	83	Centrifugation, 15 min	No	37
Highly porous activated carbon	100	0.1	900	99	Centrifugation, not available	No	38
Magnetic activated carbon	50	0.8	300	60	Centrifugation, not available	No	39
Zeolite	10	0.2	960	44	Filtration, not available	No	40
MoS_2	10	0.2	120	50	Filtration, not available	No	40
MoS_2@zeolite-5	10	0.2	240	76	Filtration, not available	Yes	40
Polymeric adsorbent	30	0.75	90	88	Not available	Yes	41
Diol-based porous organic polymers	4	0.5	90	90	Centrifugation, not available	Yes	42
FSMAS	5	0.75	10	75	Magnetic separation, 10 s	Yes	This study
FSMAS	5	0.75	240	95	Magnetic separation, 10 s	Yes	This study

regeneration rate of FSMAS decreased slightly with the increase of adsorption–desorption cycle number, probably due to the incomplete desorption of TCH molecules that adsorbed at the bottom of polymer chains and the loss of adsorbent during regeneration process. Nevertheless, after five adsorption–desorption cycles, the remained adsorption ability of FSMAS for TCH was still higher than 80%, indicating that FSMAS could be easily and effectively reused in practical application.

3.5. Comparison of adsorption performance

This novel magnetic nanoadsorbent FSMAS was compared with other adsorbents to further evaluate its application prospect. Adsorption characteristics such as adsorption efficiency, removal rate, separation ability and regeneration ability were compared in Table 3. The removal rate of TCH by FSMAS could reach 75% after only 10 minutes, and the TCH-loaded FSMAS could easily and quickly taken out from solution within 10 seconds by magnetic separation. With high adsorption efficiency, fast solid–liquid separation speed, high removal rate and satisfactory reusability, FSMAS can be used as a promising TC adsorbent.

4. Conclusions

Novel core–shell structural magnetic nanoadsorbent named FSMAS was facilely prepared by graft copolymerization of AM and SSS on the surface of vinyl-modified Fe_3O_4@SiO_2 MNPs. The graft copolymerization conditions were optimized by single factor experiments. Results showed that the maximum anionic quantity of FSMAS was achieved at initiator concentration of 1.2‰, reaction pH of 9, and monomer molar ratio of 7 : 3. The as-prepared FSMAS was fully characterized by SEM, TEM, FTIR, XPS, XRD and VSM techniques. Adsorption experiments towards TCH demonstrated that FSMAS exhibited notably higher adsorption capability than FSM in the whole tested pH range, owing to the synergistic reaction of flexible polymer

chains and abundant functional groups of P(AM-SSS). The pH-dependent adsorption capability of FSMAS indicated that electrostatic interaction, π–π stacking interaction and hydrogen bonding were involved in the adsorption process. The removal rate of TCH by FSMAS could reach 75% after only 10 minutes, and the TCH-loaded FSMAS could easily and quickly taken out from solution within 10 seconds by magnetic separation, thus significantly shortened the water treatment time. Furthermore, exhausted FSMAS was effectively regenerated by acid pickling and successfully reused in five adsorption–desorption cycles, with the remained adsorption ability towards TCH higher than 80%. All of these superior characteristics demonstrate that FSMAS is a promising adsorbent for tetracycline removal.

Author contributions

Xinyu Zheng: conceptualization, funding acquisition, investigation, methodology, validation, writing – original draft; Cong Shen: data curation, formal analysis, investigation; Yongfu Guo: resources, writing – review & editing; Huaili Zheng: funding acquisition, supervision.

Conflicts of interest

There are no conflicts to declare.

Acknowledgements

The authors are grateful for the financial support provided by the Jiangsu Education Department (No. 22KJB610023) and the Jiangsu Provincial Key Laboratory of Environmental Science and Engineering (No. JSHJZDSYS-202202). High appreciation also goes to the National Natural Science Foundation of China (No. 21677020) for the financial support.

References

1 C. Xia, H. Huang, D. Liang, Y. Xie, F. Kong, Q. Yang, J. Fu, Z. Dou, Q. Zhang and Z. Meng, Adsorption of tetracycline hydrochloride on layered double hydroxide loaded carbon nanotubes and site energy distribution analysis, *Chem. Eng. J.*, 2022, **443**, 136398.

2 G. Başkan, Ü. Açıkel and M. Levent, Investigation of adsorption properties of oxytetracycline hydrochloride on magnetic zeolite/Fe_3O_4 particles, *Adv. Powder Technol.*, 2022, **33**, 103600.

3 J. Lyu, L. Yang, L. Zhang, B. Ye and L. Wang, Antibiotics in soil and water in China – a systematic review and source analysis, *Environ. Pollut.*, 2020, **266**, 115147.

4 X. Zheng, N. Jiang, H. Zheng, Y. Wu and S. G. J. Heijman, Predicting adsorption isotherms of organic micropollutants by high-silica zeolite mixtures, *Sep. Purif. Technol.*, 2022, **282**, 120009.

5 M. Rouhani, S. D. Ashrafi, K. Taghavi, M. N. Joubani and J. Jaafari, Evaluation of tetracycline removal by adsorption method using magnetic iron oxide nanoparticles (Fe_3O_4) and clinoptilolite from aqueous solutions, *J. Mol. Liq.*, 2022, **356**, 119040.

6 L. Guardabassi, D. M. A. Lo Fo Wong and A. Dalsgaard, The effects of tertiary wastewater treatment on the prevalence of antimicrobial resistant bacteria, *Water Res.*, 2002, **36**, 1955–1964.

7 Y. Valcárcel, S. González Alonso, J. L. Rodríguez-Gil, A. Gil and M. Catalá, Detection of pharmaceutically active compounds in the rivers and tap water of the Madrid Region (Spain) and potential ecotoxicological risk, *Chemosphere*, 2011, **84**, 1336–1348.

8 R. Singh, A. P. Singh, S. Kumar, B. S. Giri and K.-H. Kim, Antibiotic resistance in major rivers in the world: A systematic review on occurrence, emergence, and management strategies, *J. Cleaner Prod.*, 2019, **234**, 1484–1505.

9 B. Turan, G. Sarigol and P. Demircivi, Adsorption of tetracycline antibiotics using metal and clay embedded cross-linked chitosan, *Mater. Chem. Phys.*, 2022, **279**, 125781.

10 X. Zheng, H. Zheng, Z. Xiong, R. Zhao, Y. Liu, C. Zhao and C. Zheng, Novel anionic polyacrylamide-modify-chitosan magnetic composite nanoparticles with excellent adsorption capacity for cationic dyes and pH-independent adsorption capability for metal ions, *Chem. Eng. J.*, 2020, **392**, 123706.

11 F. da Silva Bruckmann, C. Mafra Ledur, I. Zanella da Silva, G. Luiz Dotto and C. Rodrigo Bohn Rhoden, A DFT theoretical and experimental study about tetracycline adsorption onto magnetic graphene oxide, *J. Mol. Liq.*, 2022, **353**, 118837.

12 G. Tan, Y. Mao, H. Wang and N. Xu, A comparative study of arsenic(V), tetracycline and nitrate ions adsorption onto magnetic biochars and activated carbon, *Chem. Eng. Res. Des.*, 2020, **159**, 582–591.

13 G. Kim, Y. Yea, L. K. Njaramba, Y. Yoon, S. Kim and C. M. Park, Synthesis, performance, and mechanisms of strontium ferrite-incorporated zeolite imidazole framework (ZIF-8) for the simultaneous removal of Pb(II) and tetracycline, *Environ. Res.*, 2022, **212**, 113419.

14 W. Zhai, J. He, P. Han, M. Zeng, X. Gao and Q. He, Adsorption mechanism for tetracycline onto magnetic Fe_3O_4 nanoparticles: Adsorption isotherm and dynamic behavior, location of adsorption sites and interaction bonds, *Vacuum*, 2022, **195**, 110634.

15 C. P. Okoli and A. E. Ofomaja, Development of sustainable magnetic polyurethane polymer nanocomposite for abatement of tetracycline antibiotics aqueous pollution: Response surface methodology and adsorption dynamics, *J. Cleaner Prod.*, 2019, **217**, 42–55.

16 A. P. Tom, Nanotechnology for sustainable water treatment – A review, *Mater. Today: Proc.*, 2021, DOI: **10.1016/j.matpr.2021.05.629**, in press.

17 M. P. Ajith, M. Aswathi, E. Priyadarshini and P. Rajamani, Recent innovations of nanotechnology in water treatment: A comprehensive review, *Bioresour. Technol.*, 2021, **342**, 126000.

18 C. Lei, C. Wang, W. Chen, M. He and B. Huang, Polyaniline@magnetic chitosan nanomaterials for highly efficient simultaneous adsorption and *in situ* chemical reduction of hexavalent chromium: Removal efficacy and mechanisms, *Sci. Total Environ.*, 2020, **733**, 139316.

19 X. Zheng, H. Zheng, R. Zhao, Y. Sun, Q. Sun, S. Zhang and Y. Liu, Polymer-functionalized magnetic nanoparticles: Synthesis, characterization, and methylene blue adsorption, *Materials*, 2018, **11**, 1312.

20 Z. Wei, X. Ma, Y. Zhang, Y. Guo, W. Wang and Z.-Y. Jiang, High-efficiency adsorption of phenanthrene by Fe_3O_4-SiO_2-dimethoxydiphenylsilane nanocomposite: Experimental and theoretical study, *J. Hazard. Mater.*, 2022, **422**, 126948.

21 X. Zheng, H. Zheng, Y. Zhou, Y. Sun, R. Zhao, Y. Liu and S. Zhang, Enhanced adsorption of Orange G from aqueous solutions by quaternary ammonium group-rich magnetic nanoparticles, *Colloids Surf., A*, 2019, **580**, 123746.

22 Z. Wang, J. Xu, Y. Hu, H. Zhao, J. Zhou, Y. Liu, Z. Lou and X. Xu, Functional nanomaterials: Study on aqueous Hg(II) adsorption by magnetic Fe_3O_4@SiO_2-SH nanoparticles, *J. Taiwan Inst. Chem. Eng.*, 2016, **60**, 394–402.

23 B. Huang, Y. Liu, B. Li, S. Liu, G. Zeng, Z. Zeng, X. Wang, Q. Ning, B. Zheng and C. Yang, Effect of Cu(II) ions on the enhancement of tetracycline adsorption by Fe_3O_4@SiO_2-Chitosan/graphene oxide nanocomposite, *Carbohydr. Polym.*, 2017, **157**, 576–585.

24 W. Cai, M. Guo, X. Weng, W. Zhang and Z. Chen, Adsorption of doxorubicin hydrochloride on glutaric anhydride functionalized Fe_3O_4@SiO_2 magnetic nanoparticles, *Mater. Sci. Eng., C*, 2019, **98**, 65–73.

25 S. Zhang, H. Zheng, X. Tang, Y. Sun, Y. Wu, X. Zheng and Q. Sun, Evaluation a self-assembled anionic polyacrylamide flocculant for the treatment of hematite wastewater: Role of microblock structure, *J. Taiwan Inst. Chem. Eng.*, 2019, **95**, 11–20.

26 X. Zheng, H. Zheng, R. Zhao, Z. Xiong, Y. Wang, Y. Sun and W. Ding, Sulfonic acid-modified polyacrylamide magnetic composite with wide pH applicability for efficient removal of cationic dyes, *J. Mol. Liq.*, 2020, **319**, 114161.

27 S. K. Jana, Enhancement of photoluminescence emission and anomalous photoconductivity properties of Fe_3O_4@SiO_2 core-shell microsphere, *RSC Adv.*, 2015, **5**, 37729–37736.

28 Y. Qu, L. Qin, X. Liu and Y. Yang, Magnetic Fe_3O_4/ZIF-8 composite as an effective and recyclable adsorbent for phenol adsorption from wastewater, *Sep. Purif. Technol.*, 2022, **294**, 121169.

29 J. Miao, X. Zhao, Y.-X. Zhang and Z.-H. Liu, Feasible synthesis of hierarchical porous MgAl-borate LDHs functionalized Fe_3O_4@SiO_2 magnetic microspheres with excellent adsorption performance toward congo red and Cr(VI) pollutants, *J. Alloys Compd.*, 2021, **861**, 157974.

30 C. Zheng, H. Zheng, C. Hu, Y. Wang, Y. Wang, C. Zhao, W. Ding and Q. Sun, Structural design of magnetic biosorbents for the removal of ciprofloxacin from water, *Bioresour. Technol.*, 2020, **296**, 122288.

31 L. Feng, S. Liu, H. Zheng, J. Liang, Y. Sun, S. Zhang and X. Chen, Using ultrasonic (US)-initiated template copolymerization for preparation of an enhanced cationic polyacrylamide (CPAM) and its application in sludge dewatering, *Ultrason. Sonochem.*, 2018, **44**, 53–63.

32 L. Yi, H. Zheng, Q. Li, Y. Sun, D. Li and W. Xue, UV-initiated polymerization of hydrophobically associating cationic polyacrylamide modified by a surface-active monomer: A comparative study of synthesis, characterization, and sludge dewatering performance, *Ind. Eng. Chem. Res.*, 2014, **53**, 11193–11203.

33 Y. Liao, X. Zheng, Z. Zhang, B. Xu, Y. Sun, Y. Liu and H. Zheng, Ultrasound-assisted polymerization of P(AM-DMDAAC): Synthesis, characterization and sludge dewatering performance, *J. Environ. Chem. Eng.*, 2017, **5**, 5439–5447.

34 X. Wang, Q. Yue, B. Gao, X. Si, S. Xun and S. Zhang, Dispersion copolymerization of acrylamide and dimethyl diallyl ammonium chloride in ethanol-water solution, *J. Appl. Polym. Sci.*, 2011, **120**, 1496–1502.

35 M. E. Parolo, M. C. Savini, J. M. Vallés, M. T. Baschini and M. J. Avena, Tetracycline adsorption on montmorillonite: pH and ionic strength effects, *Appl. Clay Sci.*, 2008, **40**, 179–186.

36 Y. Zhao, J. Geng, X. Wang, X. Gu and S. Gao, Tetracycline adsorption on kaolinite: pH, metal cations and humic acid effects, *Ecotoxicology*, 2011, **20**, 1141–1147.

37 Y. Gao, Y. Li, L. Zhang, H. Huang, J. Hu, S. M. Shah and X. Su, Adsorption and removal of tetracycline antibiotics from aqueous solution by graphene oxide, *J. Colloid Interface Sci.*, 2012, **368**, 540–546.

38 D. Zhang, J. Yin, J. Zhao, H. Zhu and C. Wang, Adsorption and removal of tetracycline from water by petroleum coke-derived highly porous activated carbon, *J. Environ. Chem. Eng.*, 2015, **3**, 1504–1512.

39 R. Vinayagam, M. Quadras, T. Varadavenkatesan, D. Debraj, L. C. Goveas, A. Samanth, D. Balakrishnan and R. Selvaraj, Magnetic activated carbon synthesized using rubber fig tree leaves for adsorptive removal of tetracycline from aqueous solutions, *Environ. Res.*, 2023, **216**, 114775.

40 J. Liu, H. Lin, Y. Dong, Y. He, W. Liu and Y. Shi, The effective adsorption of tetracycline onto MoS_2@Zeolite-5: Adsorption behavior and interfacial mechanism, *J. Environ. Chem. Eng.*, 2021, **9**, 105912.

41 M. Aliyu, A. H. Abdullah and M. I. b. M. Tahir, Adsorption tetracycline from aqueous solution using a novel polymeric adsorbent derived from the rubber waste, *J. Taiwan Inst. Chem. Eng.*, 2022, **136**, 104333.

42 S. Zhang, Y. Li, C. Shi, F. Guo, C. He, Z. Cao, J. Hu, C. Cui and H. Liu, Induced-fit adsorption of diol-based porous organic polymers for tetracycline removal, *Chemosphere*, 2018, **212**, 937–945.